ANNALS OF GEOPHYSICS, 62, 1, VO09, 2919; doi: 10.4401/ag-7671

"VOLATILES AND TRACE ELEMENTS CONTENT IN MELT INCLUSIONS FROM THE ZONED GREEN TUFF IGNIMBRITE (PANTELLERIA, SICILY): PETROLOGICAL INFERENCES"

Pierangelo Romano[*,1], John C. White[2], Alessandro Ciulla[1], Ida Di Carlo[3], Claudia D'Oriano[4], Patrizia Landi[4], Silvio G. Rotolo[1,5]

(1) Dipartimento Scienze della Terra e del Mare (DiSTeM), Università degli Studi di Palermo, Palermo, Italy
(2) Department of Geosciences, Eastern Kentucky University, Richmond, USA
(3) Institut des Sciences de la Terre d'Orléans (ISTO), Université d'Orléans, Campus Géosciences, Orleans, France
(4) Istituto Nazionale di Geofisica e Vulcanologia, Sezione di Pisa, Pisa, Italy
(5) Istituto Nazionale di Geofisica e Vulcanologia, Sezione di Palermo, Palermo, Italy

Article history
Receveid **February 27, 2018**; accepted **December 18, 2018.**
Subject classification:
Melt inclusions; Zoned ignimbrite; Trachyte; Peralkaline rhyolite; Pantelleria.

ABSTRACT

The island of Pantelleria is one of the best known localities of bimodal mafic-felsic magmatism (alkali basalt and trachyte-pantellerite). Among the felsic rocks, the coexistence in a single eruption of products of both trachyte and pantellerite compositions is limited to few occurrences, the Green Tuff (GT) ignimbrite being one of these. The GT is compositionally zoned from pantellerite (70.1 wt% SiO_2, mol Na+K/Al = 1.86, 1871 ppm Zr) at the base to crystal-rich (>30 vol%) comenditic trachyte (63.4 wt% SiO_2, mol Na+K/Al = 1.10, 265 ppm Zr) at the top, although the pantellertic compositions dominate the erupted volume. We present here new data on melt inclusions (MIs) from the pantellerite portions of the GT eruption and, most importantly, from the trachyte member, which have not been studied *in-situ* by previous work focused on the GT. We document the first occurrence of trachytic melt inclusions in the late-erupted member, whose importance resides in the fact that trachytes were known mostly as crystal-rich lavas or ignimbrites, all variably affected by crystal accumulation. Besides the obvious inferences on the interplay between parental-derivative magmas, this evidence adds also some helpful elements in understanding zoning of silicic and peralkaline (i.e. low-viscosity) magma chambers. Trace elements compositions of MIs reveal that trachyte melts are of two types: (i) a *low-Ba*, directly descending from basaltic melts by 60-70 % of fractional crystallisation, and (ii) a *high-Ba* that might be affected by processes of feldspar dissolution and entrainment of the resulting small-scale melts in some MIs. MIs hosted in the deep-seated trachyte body are H_2O-poor (≤ 1.2 wt %) with respect to the early erupted (and shallower) pantellerite magma (≤ 4.2 wt %), raising the possibility that either trachyte magma was H_2O-undesaturated, or clinopyroxene hosted melt inclusions which suffered consistent H_2O loss.

1. INTRODUCTION

The Green Tuff (GT) is a low-aspect ratio rheomorphic ignimbrite that covers the island of Pantelleria (83 km^2), and is the most studied and representative eruption of the peralkaline volcano of Pantelleria. It is the caldera-forming ignimbrite of the Cinque Denti caldera and represents the last [45.7 +/- 1.0 ka, Scaillet et al., 2013] highly energetic, Plinian eruption at Pantelleria island. In the last few years several aspects of the GT have been studied in depth, including: (i) emplacement dynamics and timing of pyroclastic density currents and related hazard inferences [Williams et al., 2014]; (ii) volatile contents in melt inclusions [Lanzo et al., 2013]; (iii) phase equilibria and magma pre-eruptive conditions, derived from crystallisation experiments [Romano et al., 2018], (iv) thermodynamic petrological modelling [White et al., 2009], (v) geochronology] Scaillet et al., 2013], and (vi)

structural geology [Catalano et al., 2014].

One of the principal petrological characteristics of the GT is the continuous zoning in the peralkalinity (quantified with the Peralkalinity Index, P.I. = Na+K/Al molar ratio) of the erupted products, from the initial pantelleritic pumice fallout and the following pyroclastic currents that progressively inundated the island, to the final erupted trachytes. These latter are restricted in their areal occurrence (and volume as well) to the south west of the island.

In this paper we focus on the chemistry of melt inclusions (MIs) trapped in clinopyroxene and feldspar phenocrysts from three samples representative of the vertical chemical zoning of the GT. The rationale of our choice is in that MIs offer the possibility to avoid some pitfalls that may affect the whole rock chemistry, such as crystal accumulation/depletion, which are phenomena both widely recorded in ignimbrites, provided that melt inclusions were not modified by post-entrapment processes.

Our goals are to: (i) define the H_2O-CO_2 contents (by FTIR spectroscopy) in MIs from the trachyte products and compare the results with the volatile contents estimated in the basal pantellerite fallout, in order to trace the H_2O distribution in the GT magma chamber; (ii) characterise the trace element content in MIs; (iii) model the liquid line of descent and track the petrogenetic link between pantellerite and trachyte magmas; (iv) place some constraints on pre-eruptive conditions of the GT magma. Our final objective is to integrate all these points to explain some peculiarities of a zoned, low-temperature, peralkaline magma chamber.

2. GEOLOGICAL BACKGROUND

The Island of Pantelleria, the type locality for pantellerite magmas, is located in the continental rift of the Sicily Channel [Calanchi et al., 1989; Rotolo et al., 2006; Catalano et al., 2008], where the Moho is located as shallow as 17 km below Pantelleria [Civile et al., 2008]. Among the erupted products, alkali (ne-normative) and transitional (hy+ol-normative) basalts crop out less frequently than the felsic rocks (trachytes and pantellerites; Mahood and Hidreth, 1986), and are generally regarded as parental to the felsic magmas via low-pressure fractional crystallisation (FC) [Civetta et al., 1998; White et al., 2009; Neave et al., 2012]. Pantellerites are the dominant felsic rocks, and were emplaced in a wide variety of eruptive styles, both effusive and explosive, including strombolian, subplinian, and ignimbrite-forming eruptions (Figure 1).

The Green Tuff represents the youngest of nine ignimbrite-forming eruptions that spread over the whole island during part of island during the last 190 ka, fed by pantellerite and trachyte magmas [Jordan et al., 2018]. The on-land DRE (dense rock equivalent) volume of the GT is 0.28 km^3 [Jordan et al., 2018], a conservative estimate that must by doubled or tripled in order to take into account the amounts deposited in the sea.

One of the major peculiarities of the GT eruption with respect to the other ignimbrites emplaced on the island is its vertical chemical zonation. This reflects the progressive tapping of a compositionally zoned magma chamber from the (i) early erupted pantellerite *pumice fallout* [the 1 m thick Khartibucale member of Williams, 2010] to the (ii) *sparsely phyric Green Tuff Ignimbrite pantelleritic member* (crystal content ≤ 15 vol %), which, at the type section [8 m thick, Williams, 2010] grades into a *crystal-rich trachyte* (crystal content 20 -25 vol %) which forms the upper third of the section.

The whole eruptive sequence can be reconstructed in 2 diametrically opposed sites on the island (Figure 1) because the opening pantellerite crystal-poor pumice fallout and a large part of the following ignimbrite are preserved only in the eastern outcrops, while the topmost crystal-rich trachyte ignimbrite occurs only in a narrow sector of the west side of the island, where the type locality for the GT is also located [Williams et al., 2014].

From the bottom to the top of the sequence there is a rather continuous variation of the chemistry of whole rocks and groundmass glasses: from strongly peralkaline pantellerite to nearly metaluminous trachyte [Williams, 2010; Williams et al., 2014 and references therein] accompanied by minor variations in mineral chemistry (Na-Fe in clinopyroxene, Ca in alkali feldspar) and the occurrence of some mineral phases, whose stability is affected by the melt peralkalinity (aenigmatite, ilmenite, Fe-olivine, etc). From the petrological point of view, a general consensus exists regarding the origin of pantellerite from parental trachytes via low-pressure crystal fractionation by 70-75% removal of dominant alkali feldspar and subordinate clinopyroxene, olivine, and Fe-Ti oxides, [Civetta et al., 1998; White et al., 2009; Neave et al., 2012; Romano et al., 2018].

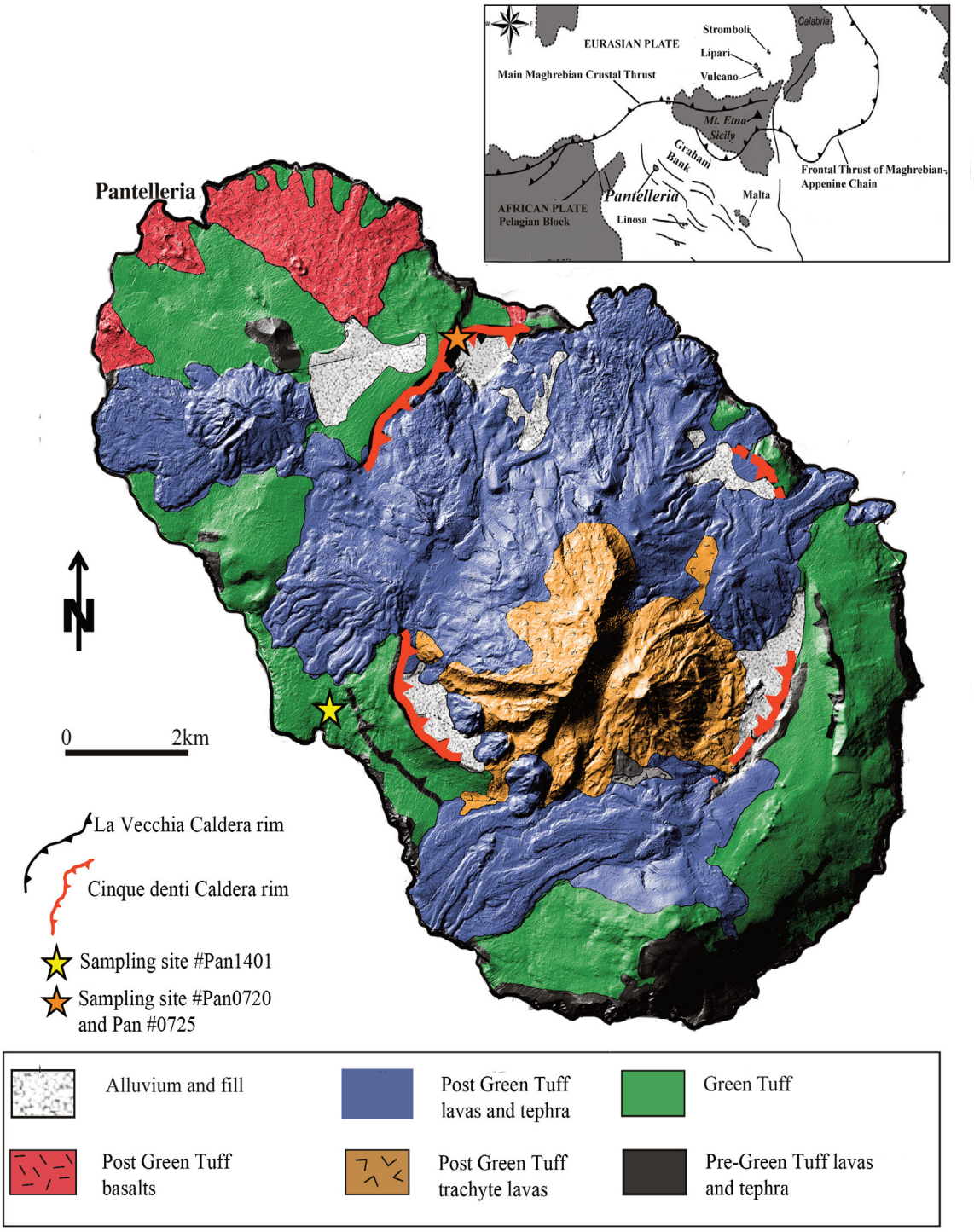

FIGURE 1. Simplified geological sketch of Pantelleria, redrawn from Scaillet et al., (2011) on a Digital Elevation Model of the island. In the inset: the island of Pantelleria within the Sicily Channel context.

3. PREVIOUS STUDIES ON VOLATILE CONTENTS IN PANTELLERITES AND ON TRACE ELEMENTS IN THE GREEN TUFF SEQUENCE

Several papers have focused on the study of melt inclusions both in basaltic rocks [Gioncada and Landi, 2010] and pantelleritic tuffs and lavas [Lowenstern and Mahood, 1991; Métrich et al., 2006; Gioncada and Landi, 2010; Neave et al., 2012] at Pantelleria, including those of Green Tuff [Lanzo et al., 2013], but studies on trachytic products have not heretofore been conducted.

Métrich et al. [2006], Gioncada and Landi [2010] and Neave et al. [2012] studied melt inclusions present in the effusive to mildly explosive eruptive units younger

than the Green Tuff and found an high H_2O (≤4.9 wt%) content, with an average value of 2.60 wt%, and CO_2 ≤150 ppm. For the Green Tuff, Lowenstern and Mahood [1991] determined a H_2O concentration of ≤1.4 wt% on reheated melt inclusions hosted in quartz and alkali feldspar phenocrysts. More recently, Lanzo et al. [2013] determined a maximum H_2Omelt content of 4.2 wt % in melt inclusions entrapped in alkali feldspar of the basal fallout, very similar to that determined in younger and much less explosive pantelleritic eruptions [Neave et al., 2012; Gioncada and Landi 2010; Metrich et al., 2006]. These concentrations were used for deriving the minimum entrapment pressures, which result close to 1.0-1.5 kbar, corresponding to a depth of around 4.0-5.5 km, decreasing to 0.6 kbar (2.5 km) for the Green Tuff feeding system.

The H_2O-rich character of pantellerite melts was independently documented by recent experimental petrology studies [Scaillet and Macdonald, 2001, 2006; Di Carlo et al., 2010]. Crystallisation experiments suggest pre-eruptive conditions for pantellerite magmas of Pantelleria as follows: T = 730-800 °C, H_2O = 4.0 wt%, P = 1.0.-1.5 kbar and fO_2 close to the FMQ buffer [Di Carlo et al., 2010].

Another import aspect revealed by studies on melt inclusions is the concentrations of other volatiles (i.e., S, F, Cl) in pantelleritic products and the consequences of their release into the atmosphere during major eruptions [Neave et al., 2012]. These volatile species are highly concentrated in pantelleritic melts: up to 590 ppm S, 4500 ppm F, and 1 wt% Cl. Unlike the other volatile elements, which increase their abundance with melt peralkalinity, Cl concentrations remain nearly constant throughout the section. Lanzo et al. [2013] hypothesised chlorine saturation in the pressure range 0.5-1.0 kbar and, accordingly with Lowenstern [1994], also a probable saturation in a mixed CO_2-H_2O vapour phase in the same pressure range.

Trace element distribution in Pantelleria lavas and tephra have been widely studied [Mahood and Stimac, 1990; Civetta et al., 1998; White et al., 2009; Neave et al., 2012 and references therein] but only recently careful attention has been paid to a detailed study of the-Green Tuff eruptive sequence [Williams, 2010; Williams et al., 2014]. Trace elements compositions of pantelleritic and trachytic matrix glasses have been first reported by Mahood and Stimac [1990] for samples representative of the bottom and top of the Green Tuff eruptive sequence. Williams [2010] analysed trace elements distributions in whole rocks and matrix glasses of closely spaced samples from the base to the top of the GT eruptive sequence. Results are broadly comparable with those reported for other pantellerites and trachytes of Pantelleria [Civetta et al., 1998; Ferla and Meli, 2006; White et al., 2009; Neave et al., 2012], namely: (i) a progressive enrichment in incompatible elements with increasing peralkalinity (i.e. from trachyte to pantellerite), (ii) an increasingly stronger negative europium anomaly with increasing peralkalinity, but with some trachytes showing a slight positive anomaly. White et al. [2009] distinguished two subgroups of trachytes on Pantelleria, (i) a *low-incompatible trace elements group* (ITE; i.e. Rb, Zr, Nb, Th), and (ii) a *high-ITE group*. These latter are also characterised by lower Ba and K/Rb and a variable Eu anomaly (Eu/Eu*= 1.14-0.64), while low-ITE trachytes, which also include the trachyte at the top of the GT, have high Ba, K/Rb and positive Eu anomalies (Eu/Eu*=1.11-1.37). In their interpretation, high-ITE trachytes are parental to pantellerites, whereas low ITE are affected by up to 40% crystal accumulation.

4. ANALYTICAL TECHNIQUES

Whole-rock analyses were performed at ALS laboratory (Camas, Sevilla, Spain), by Inductively Coupled Plasma-Atomic Emission Spectrometry (ICP-AES) and Inductively Coupled Plasma-Mass Spectrometry (ICP-MS), for major and trace element composition, respectively. Accuracy is better than 5% for all major element oxides, except CaO, MnO, and P_2O_5 (14%), and better than 8% for all trace elements except Nb (<30%).

Major element composition and Cl, F, S of MI were analysed by electron microprobe (CAMECA SX-Five at Institut des Sciences de la Terre d'Orleans) using an acceleration voltage of 15 kV, sample current 6 nA and counting time of 10 s on peak and background for all elements; Na and K were analysed first and a ZAF correction was applied. Mineral phases were analysed using a focused beam, while melt inclusions were analysed using a 5 to 10 µm defocused beam in order to prevent Na migration.

Trace elements in MIs were analysed by *Laser Ablation Inductively Coupled Plasma Mass Spectrometry* (LA-ICP-MS) (GeoLasPro 193 nm ArF Excimer laser ablation (LA) system, connected with an Agilent 7500ce quadrupole ICP-MS at Istituto Nazionale di Geofisica e Vulcanologia, Sezione di Palermo) using a Laser repe-

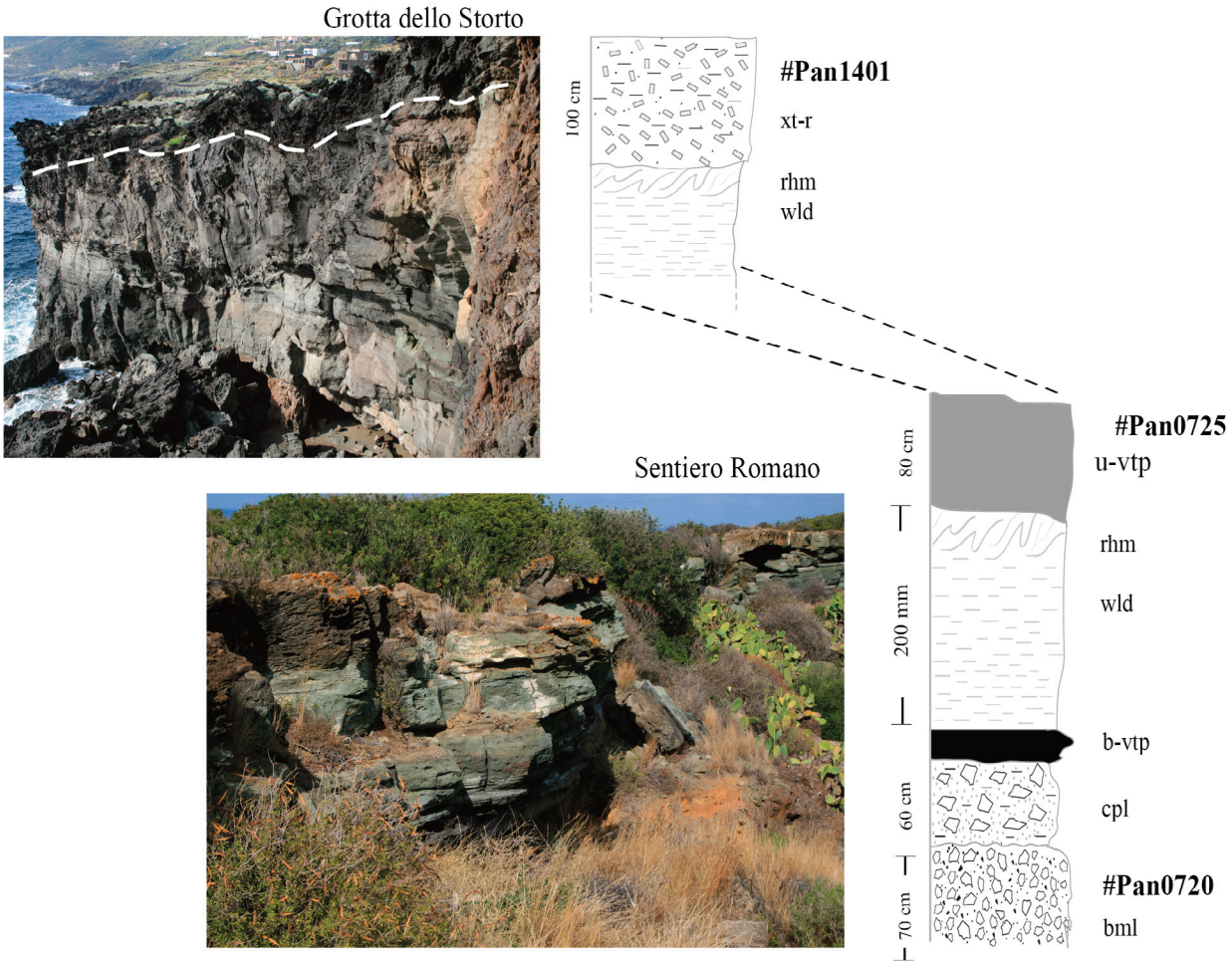

FIGURE 2. General view and schematic stratigraphic sections of the sampled sites of the Green Tuff. At Grotta dello Storto, the crystal-rich portion of GT (*xt-r*) overlays the rheomorphic (rhm) and welded (wld) lithofacies. At Sentiero Romano, the GT section includes a massive basal pumice fallout (*bml*), followed by a pumice flow (*cpl)*, then the basal vitrophyre (*b-vtp*) overlaid by the welded (wld) and rheomorphic (rhm) portion of GT, and the upper vitrophyre (u-vtp) that closes the sequence.

tition rate of 10 Hz, a spot size between 24 and 32 µm, corresponding to a Fluency between 14 and 15.5 J cm^{-2}, respectively, and a flux of He in the ablation cell ranging between 0.82-0.79 L/min. Data acquisition was accomplished in peak-jumping mode with a dwell time of 10 ms. Plasma conditions were adjusted to oxide formation <0.2%, monitored using the 248/232 mass ratio. For each melt inclusion, one or two spots (where there was enough space), were performed, each spot analysis lasting 2 minutes, including 60sec for background acquisition and 60 sec for the analysis.

NIST RM 612 and ^{43}Ca (from EMPA) were adopted as external and internal standards, respectively. Accuracy of analyses (RSD%), checked by repeated measurements of the USGS basaltic reference glass BCR-2G, results between 0-5 % for Sc, La, Ce, Eu, Th, U, Pb, Ta, Nd, Cr, Ba, Gd, Pr, Sr, Yb; 6-10% for Co, Nb, V, K, Hf, Lu, Sm, Er, Ho, Dy and 11-18% for Zn, Y, Zr, Rb, Cs, Tm, Ti and Li.

The determination of water content in the selected melt inclusions of GT trachytic member was carried out using a Fourier Transform Infrared (FT-IR) spectroscopy using a Bruker Hyperion 2000 FT-IR spectrometer coupled with a microscope (fluxed with CO_2- and H_2O-free compressed air) housed at DiSTeM, University of Palermo. Feldspar and clinopyroxene phenocrysts in the size range 250-500 microns were hand-picked from crushed rock samples, mounted in Crystal Bond™ and double polished (reduced to wafers 30-100 µm thick) to expose melt inclusions at the surface, and finally mounted on a ZnSe disk for FT-IR analysis. Sample spectra and background were acquired in the 1000-6000 cm^{-1} absorption range with a resolution of 2 cm^{-1}, adopting a Globar source with a

Sampe ID	lithofacies	Sampling site	Coordinates	Phenocrysts
PAN 0720	basal pumice fallout	Roman Road	36°49'10.25''N 11° 50'45.86''E	afs > aenig >cpx > ol, qz
PAN 0725	intermediate vitrophire	Roman Road	36°49'10.25''N 11°50'45.86''E	afs > aenig > cpx +/- qz
PAN 1401	top crystal-rich trachyte	Grotta dello Storto	36°46'19.02''N 11°57'22.97E	afs > cpx > ol > Fe-Ti ox

TABLE 1. Sample location and mineralogy. Afs= (Na, K) feldspar, aenig= aenigmatite, cpx= clinopyroxene, Fe-Ti ox= Fe-Ti oxides, ol= olivine, qz= quartz

MCT detector and scan rate of 20 kHz and completing 256 scans.

Water concentrations were derived from total H_2O absorption band (3550 cm^{-1}) using a straight baseline correction [TT method in Ohlhorst et al., 2001] and applying the Beer-Lambert equation, $c = (MW*A)/(d*\rho*\varepsilon)$, where c is the wt% of dissolved H_2O, MW the molecular weight of H_2O, A the height of the absorption peak, d the sample thickness in cm, ρ the glass density in g L^{-1}, ε the molar extinction coefficient. The glass density (2410 g L-1) was calculated according to the Ochs and Lange [1999] algorithm, considering the average composition of glass inclusions. The adopted molar extinction coefficient (ε^{3550}) was 64 L mol^{-1} cm^{-1} [Dixon et al., 1995].

5. SAMPLES DESCRIPTION

The samples selected for this study (Table 1, Figure 2) are representative of the Green Tuff intra-eruptive chemical and petrographic variability. From the top to the bottom of the sequence, three samples were analysed:

(i) the poorly studied topmost trachyte ignimbrite (sample # PAN 1401), (ii) the immediately lower (although outcropping in a different section) upper vitrophyre of the pantelleritic ignimbrite (sample # PAN 0725) and (iii) the basal pumice fallout (sample # Pan 0720) of the GT.

The basal pumice fallout (# Pan 0720) was sampled at the Roman Road site (Figure 1) and consists of 70-80 cm thick pumice lapilli with scarce lithic fragments (<2 cm long) that increase slightly in abundance upwards. Pumice crystallinity is <10 vol% and the mineral assemblage is dominated by alkali feldspar (Ab_{65}-Or_{35}), clinopyroxene ($Wo_{38}En_9Fs_{40}Aeg_9$), aenigmatite, fayalite (Fa_{88-91}), ilmenite and quartz.

The blackish intermediate vitrophyre (# Pan 0725), although stands at the top of the GT sequence at Sentiero Romano, in the general stratigraphy (compiled in two sites, Figure 2), is positioned just below the crystal-rich trachyte. The vitrophire is a ca. 80 cm thick layer, with crystallinity up to 15 vol%, slightly higher with respect to the lower portions of the GT ignimbrite (typically pistachio-green in colour). Mineral abundance and composition are similar to Pan 0720, with the absence of olivine.

The topmost phenocryst-rich trachyte (# Pan 1401) was sampled at Grotta dello Storto (2 km SW from the type section of Williams, 2010), it is a > 2-m thick welded tuff. Mineral assemblage consists of about 30 vol% of dominant alkali feldspar ($Ab_{70}Or_{25}$ An_5), followed by clinopyroxene ($Wo_{42-43}Fs_{28-30}En_{27-29}$), olivine ($Fa_{72-86}$), magnetite (usp =71 mol%), ilmenite (hem = 5 mol%). Feldspar phenocrysts (up to 15 mm long) often show sieve textures coupled to surfaces of resorption and re-growth close to the crystal rims, but without any relevant core to rim chemical variation

6. RESULTS

The basal and intermediate samples have pantelleritic composition with SiO_2= 70.1 wt%, Na_2O + K_2O= 10.7 wt%, and P.I. =1.86, and minor variations in the average trace element contents (Zr= 1871 ppm, La= 89 ppm, Rb= 145 ppm, Nb= 457 ppm, Ba= 289 ppm, Sr= 3 ppm). The topmost trachyte has SiO_2= 63.4 wt%, Na_2O+K_2O=11.4 wt%, P.I.=1.1, lower contents of incompatible trace elements (Zr= 265 ppm, La= 48 ppm, Rb= 36 ppm, Nb= 70 ppm) and relatively high contents of compatible trace elements (Ba= 1720 ppm, Sr= 56 ppm). REE pattern shows an evident positive Eu anomaly (Eu/Eu* = 1.61).

6.1 MELT INCLUSIONS TEXTURES AND COMPOSITIONS

More than 350 crystals-hosting MI were selected for this study. Alkali feldspar crystals were selected in the intermediate pantelleritic sample, while for the topmost trachytic member only clinopyroxene crystals were used, because MIs in alkali feldspar (heavily fractured) and olivine phenocrysts were entirely crystallised and thus useless for our purposes. The same MIs analysed for major elements and volatiles in the basal fallout by Lanzo et al. [2013] were used here for trace element analyses.

Textures of MIs trapped in alkali feldspars of the basal fallout and vitrophyre (PAN 0725) are usually subspherical to ovoid and can reach dimension up to 600 µm (Figure 3). The analysed melt inclusions are entirely glassy and those presenting shrinkage bubbles, hourglass shapes or daughter minerals (usually clinopyroxene), all evidences of post entrapment modifications, were discarded.

MIs in the phenocrysts from the upper trachytic member are generally scarce and relatively small, thus although about 200 clinopyroxene were analysed it was only possible to select a few MIs suitable for water and trace elements analyses. Trachyte MIs have a spherical or sub-spherical shape and range from 20 to 200 µm in diameter. Tiny Fe-Ti oxides were commonly found at the rim of the inclusions, sometimes coupled with shrinkage bubbles (Figure 3).

Major elements compositions of MIs do not show significant variations between the two pantellerite samples (Table 2). Compositions of pantellerite MIs have a limited range of variation: SiO_2 between 69.5-72.6 wt%, $Na_2O + K_2O$ between 9.5 and 11.0 wt%, Al_2O_3 between 8.5-9.6 wt% and FeO_{tot} between 7.2-7.8 wt%; all other major element oxides are < 1 wt%. Melt inclusions from the upper trachyte have SiO_2 = 63.1 - 66.0 wt%, with N_2O+K_2O = 11.9 – 13.0, Al_2O_3 up to about 14.8 wt%,

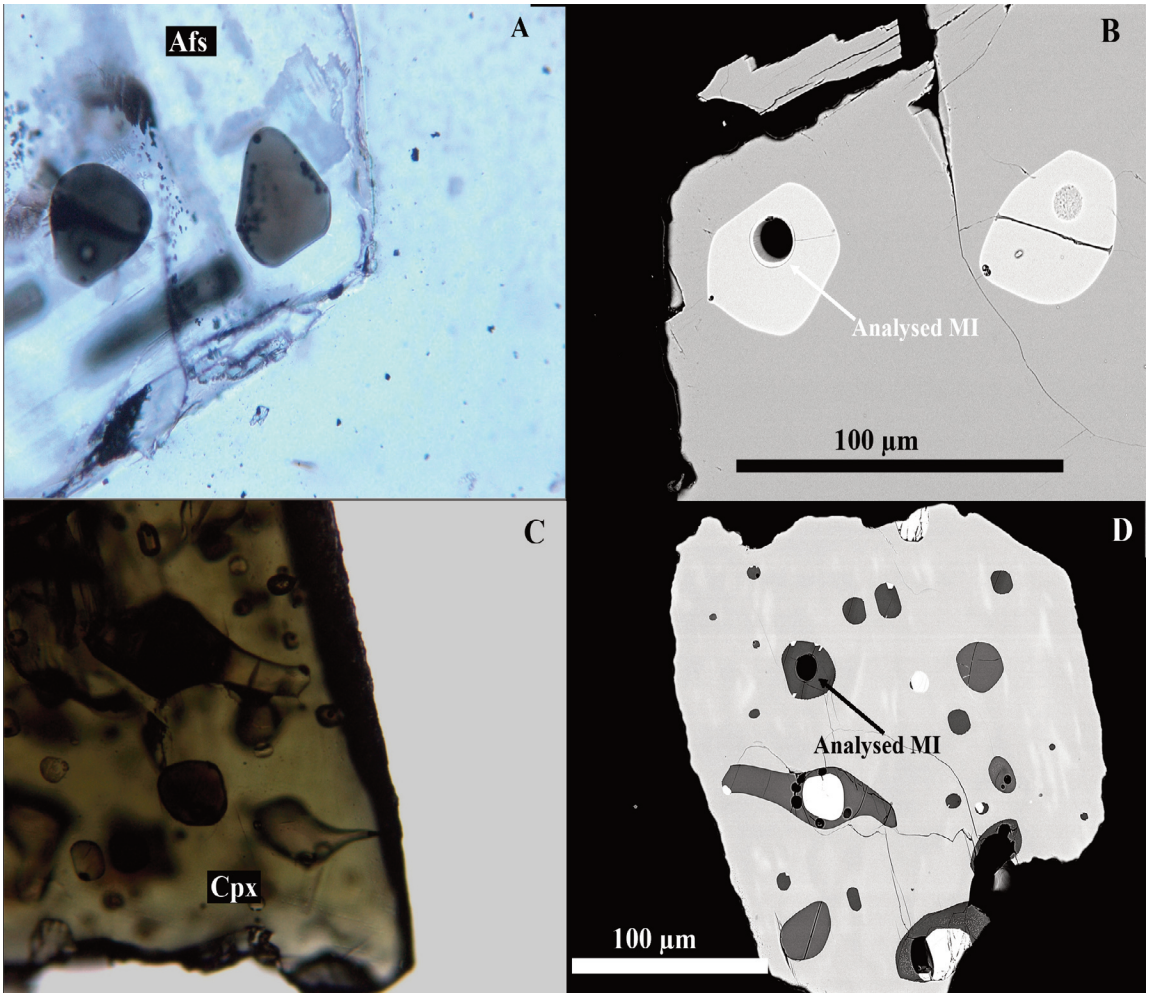

FIGURE 3. Microphotos and SEM images of analysed melt inclusions: (A) microphoto (parallel polars) of the melt inclusions trapped in alkali feldspar (Afs) of sample # Pan0725; (B) SEM BSE image of the same MI shown in (A) with the LA spot. (C) microphoto (parallel polars) of the melt inclusions trapped in clinopyroxene (cpx) (sample #Pan1401); (D) SEM-BSE image of the same MI shown in (C) with the LA spot.

Sample	Pan 1401 (39) 1	Pan 1401 (40) 1b	Pan 1401 (47)1	Pan 1401 (46) 1	Pan1401 (47)1	Pan 1401 (47) 2
SiO_2 wt %	61.37	62.71	63.47	64.72	64.39	64.46
TiO_2	0.89	0.90	0.85	0.85	0.86	0.78
Al_2O_3	13.40	13.72	14.06	14.53	14.18	13.89
FeO_{tot}	6.54	5.20	4.57	3.79	5.26	4.85
MnO	0.19	0.21	0.20	0.19	0.21	0.15
MgO	0.45	0.36	0.22	0.22	0.25	0.23
CaO	1.09	1.03	0.90	0.64	1.17	0.96
Na_2O	7.70	6.97	7.69	7.37	7.43	7.66
K_2O	4.80	4.53	4.93	5.03	4.86	4.76
P_2O_5	0.11	0.20	0.10	0.30	0.20	0.24
Cl			0.13	0.09		
F			0.01	0.17		
SO_2			0.10	0.09		
BaO			0.20	0.11		
Total	**96.55**	**95.83**	**96.98**	**97.62**	**98.80**	**97.98**
Cs ppm	0.42	0.38	0.35	0.26	0.33	0.45
Rb	49	46	45	39	43	57
Ba	945	1341	897	1182	1308	1021
Th	5.0	4.6	4.0	3.5	5.3	5.2
U	1.63	1.64	1.46	1.29	1.98	1.94
K	43618	45207	42388	38275	44923	51004
Nb	89	87	80	72	91	97
Ta	5.0	4.9	4.6	4.2	5.4	5.6
La	52	52	44	39	55	54
Ce	114	120	101	88	124	122
Pb	2.8	2.8	3.0	2.6	3.4	3.6
Pr	12.6	13.6	11.1	9.8	13.5	13.5
Sr	22.6	13.0	22.0	24.9	22.6	10.6
Nd	52.1	55.1	43.9	38.4	56.0	55.3
Zr	252	240	218	194	258	268
Hf	6.2	5.4	5.1	4. 9	6.6	6.2
Sm	10.5	10.4	8.7	7.5	11.2	11.1
Eu	3.7	4.6	3.2	3.3	4.3	4.5
Gd	9.8	9.7	7.9	6.5	9.5	9.4
Tb	1.29	1.42	1.12	0.99	1.32	1.36
Dy	8.0	7.9	6.5	5.4	8.3	8.6
Ho	1.5	1.4	1.2	1.1	1.5	1.6
Y	37	37	31	26	37	40
Er	3.9	4.0	3.3	2.4	4.1	4.2
Tm	0.55	0.51	0.49	0.41	0.58	0.61
Yb	3.7	3.9	2.8	2.7	4.0	4.00
Lu	0.57	0.58	0.46	0.34	0.59	0.51
FeO_{tot} = total iron reported as FeO.						

TABLE 2. Major (EMP) and trace element (ppm) composition of melt inclusions of the samples: #Pan1401, #Pan0725 and #Pan0720.

and FeO_{tot} between 4.3 -7.5 wt%. Average P.I. in the pantellerite MIs is 2.11 ± 0.23 and is 1.2-1.3 in the trachyte MIs. Pantellerite-hosted melt inclusions also classify as pantellerite, and trachyte-hosted MIs classify as comenditic trachyte [Macdonald, 1974; Figure 4].

Melt inclusions from the two pantellerite samples (Table 2, Figure 5) are strongly enriched in incompatible trace elements (Zr= 1546-1997, Nb=354-447, Y= 154 -193 ppm), a typical feature of pantellerite melts. Primitive mantle-normalised REE patterns show an en-

Sample	Pan 0725 (1)	Pan 0725 (2)	Pan 0725 (3)	Pan 0725 (4) 1	Pan 0725 (4) 2	Pan 0725 (5) 1
SiO_2 wt %	64.71	66.03	67.17	66.74	67.83	67.05
TiO_2	0.48	0.72	0.36	0.43	0.44	0.61
Al_2O_3	6.56	6.91	7.01	7.21	7.38	6.92
FeO_{tot}	8.26	9.10	9.16	7.80	8.30	8.81
MnO	0.22	0.54	0.31	0.49	0.25	0.28
MgO	0.08	0.18	0.14	0.13	0.14	0.20
CaO	0.30	0.54	0.39	0.32	0.33	0.58
Na2O	6.32	6.65	6.42	4.25	6.40	6.45
K_2O	4.25	4.26	4.38	4.54	4.31	4.07
P_2O_5	0.00	0.00	0.07	0.05	0.00	0.03
Cl	1.01	1.06	1.01	0.94		
F				0.40		
SO_2						
BaO						
Total	**92.19**	**95.99**	**96.42**	**91.96**	**95.37**	**95.00**
Cs ppm	2.7	2.3	2.4	2.6	2.6	2.9
Rb	229	175	186	214	217	223
Ba	45	63	51	43	45	93
Th	36.4	32.9	31.8	35.6	34.3	37.9
U	12.27	11.00	10.89	11.82	11.34	12.90
K	40580	34512	35477	39486	39979	42203
Nb	410	358	355	384	402	448
Ta	25.5	23.3	22.1	25.1	24.6	27.0
La	227	204	195	211	221	236
Ce	450	398	395	433	444	481
Pb	16.8	15.1	14.9	16.4	15.7	18.7
Pr	46.6	41.9	39.8	44.0	45.7	49.2
Sr	2.3	3.7	2.8	2.1	2.3	5.1
Nd	173	155	148	161	169	178
Zr	1795	1609	1546	1648	1721	1859
Hf	43	40	38	41	42	45
Sm	32	29	28	31	31	33
Eu	4.7	4.7	4.2	4.6	4.6	6.0
Gd	32	28	26	28	30	32
Tb	4.8	4.3	4.2	4.4	4.6	5.0
Dy	31	28	28	28	30	32
Ho	6.4	5.8	5.3	5.8	6.0	6.4
Y	164	145	139	153	156	164
Er	18	17	15	17	17	18
Tm	2.6	2.4	2.3	2.5	2.5	2.5
Yb	17.5	16.4	15.3	17.4	16.6	18.6
Lu	2.5	2.2	2.2	2.3	2.4	2.6

TABLE 2. Continued.

richment in LREE over HREE (La_N/Lu_N = 9.0- 9.6 and Ce_N/Yb_N = 6.0 -7.0) and a pronounced negative Eu anomaly (Eu/Eu* = 0.44 - 0.56), while Ba and Sr are low to extremely low, respectively; these selective depletions are consistent with the high degree of feldspar fractionation required to originate pantelleritic rocks [Civetta et al., 1998; White et al., 2009]. The most evident difference in the trace elements distribution between the basal fallout and the upper vitrophyre is a slight decrease in incompatible trace element concentrations in MIs from the latter.

On the basis of the Ba content, MIs trapped in pyroxene from GT trachyte are bimodal in composition. It is possible to distinguish two groups, referred as (i) *low-*

Sample	Pan 0720 (5)	Pan 0720 (6)	Pan 0720 (10)	Pan 0720 (11)	Pan 0720 (12)	Pan 0720 (15)	Pan 0720 (17	Pan 0720 (24)
SiO_2 wt %	69.01	69.40	69.21	68.73	68.13	68.87	69.06	68.85
TiO_2	0.70	0.56	0.45	0.54	0.58	0.50	0.55	0.68
Al_2O_3	7.10	7.35	7.19	7.23	7.10	7.20	7.36	7.27
FeO_{tot}	8.79	8.11	8.38	8.26	8.98	7.89	8.44	8.52
MnO	0.37	0.29	0.35	0.39	0.39	0.33	0.37	0.34
MgO	0.17	0.12	0.17	0.14	0.19	0.13	0.19	0.15
CaO	0.55	0.40	0.44	0.48	0.70	0.30	0.43	0.44
Na_2O	6.55	6.36	6.73	6.37	6.61	6.38	6.77	6.53
K_2O	3.82	3.85	3.84	3.81	3.80	3.91	3.92	3.79
P_2O_5	0.06	0.04	0.04	0.05	0.05	0.02	0.05	0.04
Cl	1.05	1.01	1.04	1.05	1.04	1.04	1.01	1.02
F	0.24	0.19	0.25	0.28	0.21	0.23	0.22	0.13
SO_2	0.08	0.08	0.08	0.09	0.08	0.06	0.08	0.09
BaO								
Total	**98.47**	**97.76**	**98.17**	**97.43**	**97.84**	**96.87**	**98.45**	**97.86**
Cs ppm	2.4	2.6	2.6	2.5	2.3	2.6	2.5	2.5
Rb	191	201	200	202	184	202	203	200
Ba	67	62	63	55	80	50	52	58
Th	34.5	41.9	38.3	39.2	37.5	37.6	37.3	39.6
U	12.18	13.42	12.22	12.35	11.90	11.89	12.06	12.23
K	36100	36908	37181	38181	36472	36411	36831	37874
Nb	390	414	404	399	384	391	390	396
Ta	24.1	28.5	26.5	26.2	25.2	25.3	25.0	25.8
La	220	252	242	243	227	236	234	256
Ce	442	495	469	470	442	454	446	459
Pb	16.6	18.0	16.8	16.5	15.7	16.0	16.3	16.7
Pr	46.0	52.3	49.8	49.9	46.8	47.6	47.3	51.8
Sr	3.9	3.7	3.5	3.1	4.6	2.7	2.9	3.4
Nd	164	193	180	178	170	172	172	188
Zr	1661	1917	1882	1897	1840	1874	1826	1997
Hf	41	51	47	48	47	46	46	49
Sm	31	38	35	34	32	34	33	37
Eu	5.1	5.7	5.4	5.1	5.2	4.9	4.8	5.4
Gd	30	36	34	34	32	33	33	35
Tb	4.6	5.4	5.2	5.2	4.8	5.1	5.0	5.4
Dy	30	36	34	34	32	34	33	35
Ho	5.9	7.1	6.7	6.8	6.3	6.7	6.5	7.1
Y	154	179	178	181	169	180	174	194
Er	17	20	19	20	18	19	19	20
Tm	2.5	3.0	2.9	3.0	2.7	2.8	2.7	3.0
Yb	16.8	20.7	19.2	19.4	18.1	18.7	18.3	20.0
Lu	2.4	2.9	2.7	2.7	2.6	2.7	2.6	2.9

TABLE 2. Continued.

Ba (Ba 897-1021 ppm) and (ii) *high-Ba* (1183-1341 ppm). Although less enriched, the REE patterns of MIs from the GT trachyte result similar to pantellerites (La_N/Lu_N = 9.3- 11.1 and Ce_N/Yb_N = 8.0-9.4), apart for a well-developed positive Eu anomaly (1.10 – 1.42, mean = 1.27 +/- 0.13). More in detail, melt inclusions of the GT trachyte are characterised by a minor degree of enrichment in incompatible elements such as Rb (39-57, mean = 46 ppm), Y (26-40, mean=35 ppm), Zr (194-267, mean=238 ppm), Nb (72- 98, mean=86 ppm) and higher Ba (897-1341, mean= 1116 ppm) and Sr (11-25, mean= 20 ppm), with respect to GT pantellerite melt inclusions (Figure 5).

These geochemical features differ also from the

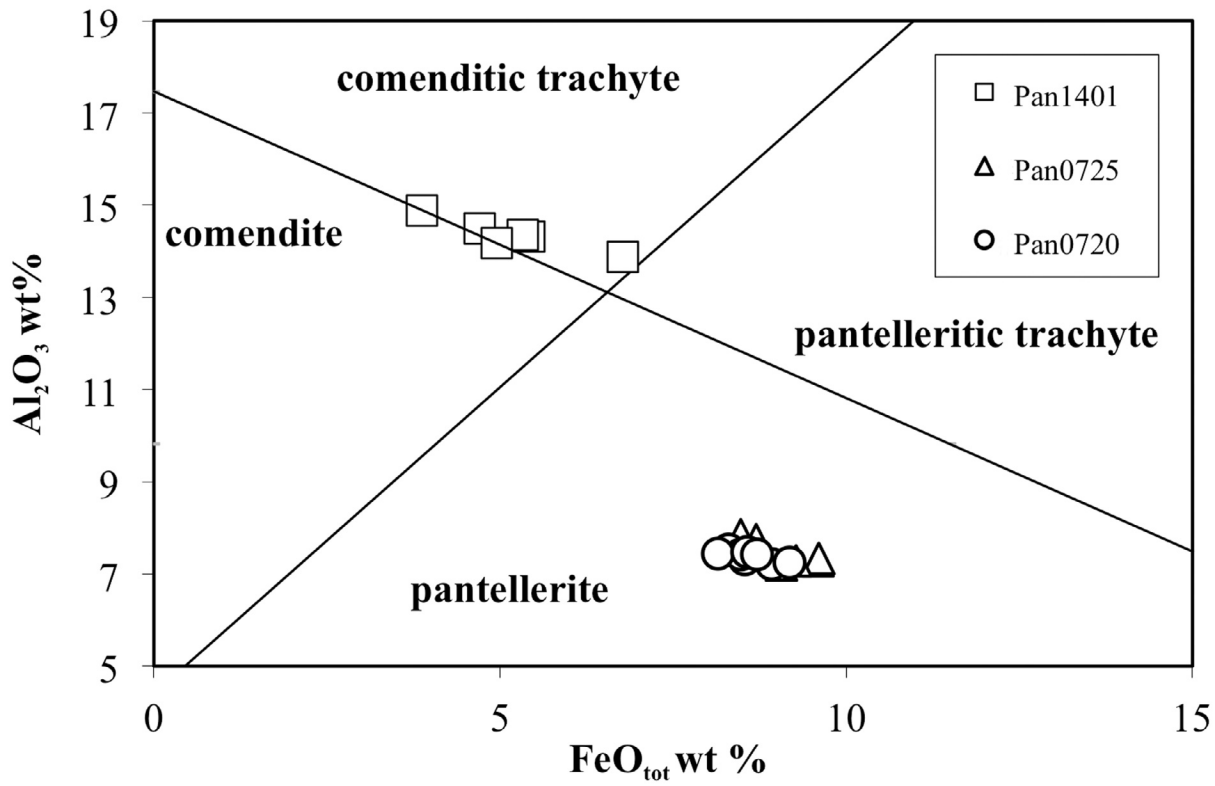

FIGURE 4. Composition of melt inclusion analyses plotted in the classification diagram FeO_{tot} vs Al_2O_3 for peralkaline rocks [Macdonald, 1974]. Squares: melt inclusions of sample Pan1401, triangles: melt inclusions of sample Pan0725; circles: melt inclusions of sample Pan0720.

other Pantescan trachytes (whole rock analyses) erupted on the island during the last 50 ka, in terms of both compatible (Sr and Ba) and incompatible (Th, Rb, Zr) elements.

6.2 VOLATILE CONTENT

Water contents were determined on 14 melt inclusions trapped in clinopyroxene phenocrysts ($Wo_{42-43}Fs_{28-30}En_{27-29}$) of the GT trachytic member. The dissolved H_2O content ranges from 0.15 to 1.05 wt%, with an average of 0.73 ± 0.2 wt% (Table 3). CO2 was always below the detection limit of the FT-IR spectroscopy (50 ppm). Surprisingly, the water content hence results much lower than that determined by Lanzo et al. [2013] in the melt inclusions from the basal fallout.

As regards the other volatiles (Cl, F, S) content, Cl content in the trachytic MIs is in the range 600 - 1500 ppm (mean= 1150 +/- 200), F ranges from 100 to 3000 ppm, S between 300 and 1500 ppm. In pantelleric melt inclusions of the top vitrophyre, chlorine content is close to 1 wt %, similarly to the maximum Cl content measured in the basal fallout [Lanzo et al., 2013], while the average S content is 500 ppm.

LAB number	A_{3550}	T (µm)	H_2O_{tot}
Cir (a)	0.140	35	0.47
Cir (b)	0.160	35	0.53
F	0.232	26	1.04
Zam-1	0.200	28	0.83
Zam-2	0.230	28	0.96
7	0.168	55	0.36
8a	0.197	30	0.77
8b	0.171	30	0.67
9a	0.201	45	0.52
31a	0.090	70	0.15
36a	0.225	25	1.05
45a	0.191	32	0.70
Zab	0.194	36	0.63
18	0.248	40	0.72
zag	0.131	25	0.61

TABLE 3. FT-IR analyses of water content in clinopyroxene-hosted melt inclusions of sample #Pan1401 (top trachyte). A_{3550} = absorbance at the fundamental absorption band; (H_2O_{tot}, 3550 cm^{-1}) T = thickness of MI. nd=not detected. CO_2 (CO_3^{--}) was always below detection limits (<50 ppm).

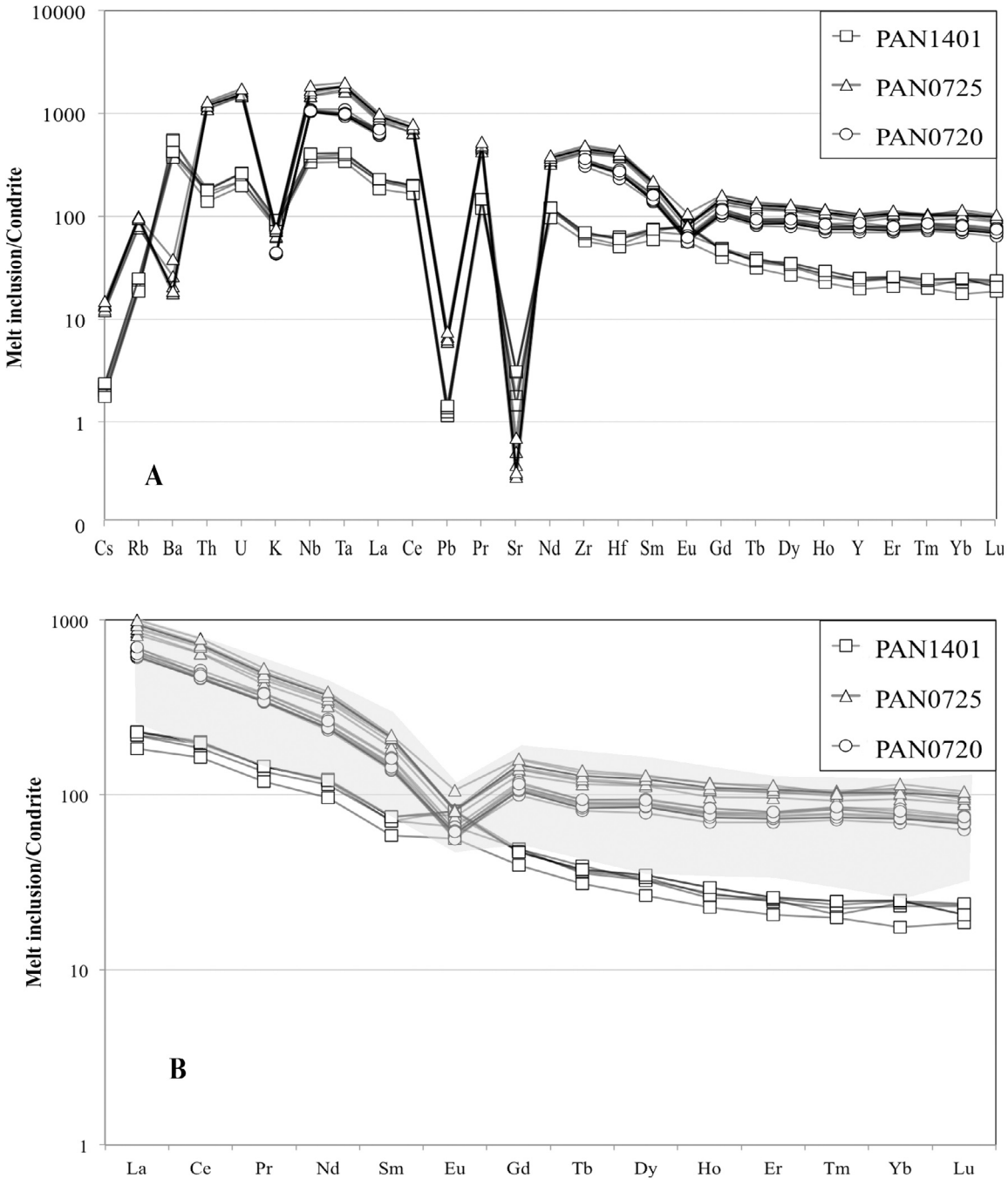

FIGURE 5. (A) Spider diagram for melt inclusions analysed in this work. Symbols as in Figure 4. (B) Rare earth element patterns of melt inclusions normalised to chondrite [normalisation values from McDonough and Sun, 1995]. The grey-field represents the rare earth elements pattern of felsic rocks and glasses of other Pantelleria samples, reported in Civetta et al., [1998], White et al., [2009], Neave et al., [2012].

7. DISCUSSION

The innovative aspect of this paper is the discovery of melts inclusion in the trachytic products from Pantelleria, which can provide a new element in the study of the petrogenetic evolution of the peralkaline magmas at Pantelleria. In fact, previous studies have utilised whole rock or glass and mineral data for discussing the genetic origin of trachytes from basalts, and pantellerite from trachyte [Civetta et al., 1998; White et al., 2009]. These works used lavas and tuffs that may have followed very similar liquid lines of descent, but belong to several different eruptive cycles over the past 45 ka. Conversely, all our samples belong to the GT eruptive

sequence, which actually represents a single chemically zoned magma body. The composition of MIs shows a narrow range of variation, and they are considered unmodified by post entrapment crystallisation (PEC) of the host mineral (cpx) since the amount of crystallisation estimated is lower than 3%, on the basis of the abundances of Sc (compatible in cpx), Sm and Zr (incompatible in cpx) from the less to the more evolved terms. This suggests that MIs represent the composition of the original trachytic melt.

7.1 MAJOR AND TRACE ELEMENT MODELS

Major element models of the petrogenesis of comenditic trachyte to pantellerite at Pantelleria have been performed by several previous workers [Civetta et al., 1998; White et al., 2009; Neave et al., 2012]. In particular, White et al., (2009) modelled the evolution of a pantellerite lava (Sciuvechi, P.I. = 1.91, Zr = 2301 ppm) from comenditic trachyte inclusions in the Khaggiar flow (P.I. = 1.12, Zr = 583 ppm), suggesting a significant role for *alkali feldspar* (85% of the fractionating assemblage), and in minor amount of clinopyroxene (~10%), olivine (~4%), ilmenite (~1%), and apatite (<1%), to originate a pantellerite melt from a trachyte parent by fractional crystallisation.

We present a two-step major element mass balance and a trace element model for the differentiation of alkali basalt to GT comenditic trachyte, then to GT pantellerite (Table 4). Sample 060534 [White et al., 2009] was selected as the model alkali basalt parent, MI Pan1401(46)1 as the comenditic trachyte differentiate (P.I. = 1.23, Zr = 194 ppm) and MI Pan0725(1) as the pantelleritic daughter (P.I. = 2.28, Zr = 1859 ppm). Major elements mass balance modelling suggests that the relatively most primitive trachytic MIs can be derived from basalts through ~73% fractionation of an assemblage dominated by plagioclase (~42%) and clinopyroxene (~33%), with subordinate magnetite (~15%), olivine (~8%), and apatite (~3%). The relatively most evolved pantellerite MIs can then be derived by ~73% fractionation of an assemblage dominated by anorthoclase (~96%), with minor (<2% each) ilmenite, clinopyroxene, olivine, and apatite. Major element mass balance modelling [this work, Civetta et al., 1998; White et al., 2009] and principal component analysis [Neave et al., 2012] agree in indicating that the alkali feldspar fractionation (≥ 75wt%) plays a dominant role on the origin of pantellerites from trachytes, both for the Green Tuff and others eruptions. To the contrary, mafic phase (i.e clinopyroxene, Fe-Ti oxides, olivine, amphibole, aenigmatite) contribute to the crystallising mineral assemblage in a less clear way, probably being responsible of the slightly differences observed among the pantelleritic melts.

Trace element modelling was performed using the results of mass balance calculations and mineral/liquid partition coefficients presented by Neave et al. [2012] for Step 1 (from alkali basalt to comenditic trachyte), and by Mahood and Stimac [1990] for Step 2 (from comenditic trachyte to pantellerite). These models suggest that the comenditic trachyte MIs may be formed after 60-70% of fractional crystallisation, and pantelleritic MIs after an additional 85-90% fractional crystallisation (Figure 6).

High Ba concentrations (898-1308 ppm) and positive Eu anomalies [$Eu/Eu^* = 1.12$-1.46, values normalised to CI chondrite, following McDonough and Sun, 1995] are features observed in all the trachytic MIs from GT and were likely inherited from the original geochemical characteristics of parental basalts which show positive Eu anomalies and high LILE concentrations [Civetta et al., 1998; White et al., 2009]. However, the very high Ba concentration (> 1100 ppm) could be explained invoking processes of crystal accumulation, as commonly suggested for whole rocks chemistry of products of similar composition [i.e. White et al., 2009; D'Oriano et al., 2017]. In fact, modelling the addition of about 10% of alkali feldspar to low Ba-trachytic liquids we obtained Ba contents comparable with that of high-Ba trachytic liquid. This could be explained with a batch melting of an alkali feldspar cumulate mush or alternatively entrapment within clinopyroxene of very local (micro-scale) melts due to partial dissolution of feldspar phenocrysts. Comparison with the whole-rock analyses from GT type section clearly shows that comenditc trachyte samples with Ba > ~1300 ppm have been affected by concomitant processes of crystal accumulation (Figure 6A). The occurrence of variable lobate to ovoid feldspar phenocrysts with sieve to hollow textures might provide textural evidence that some dissolution of feldspars could have taken place before the eruption.

7.2 P-T-H_2O PRE-ERUPTIVE CONDITIONS

The pre-eruptive magma conditions were estimated using the composition of Ti-magnetite and ilmenite pairs in the studied products. One analysis of ilmenite (#1401b-10) in the upper trachytic sample is in equilibrium with four analyses of magnetite, following the cri-

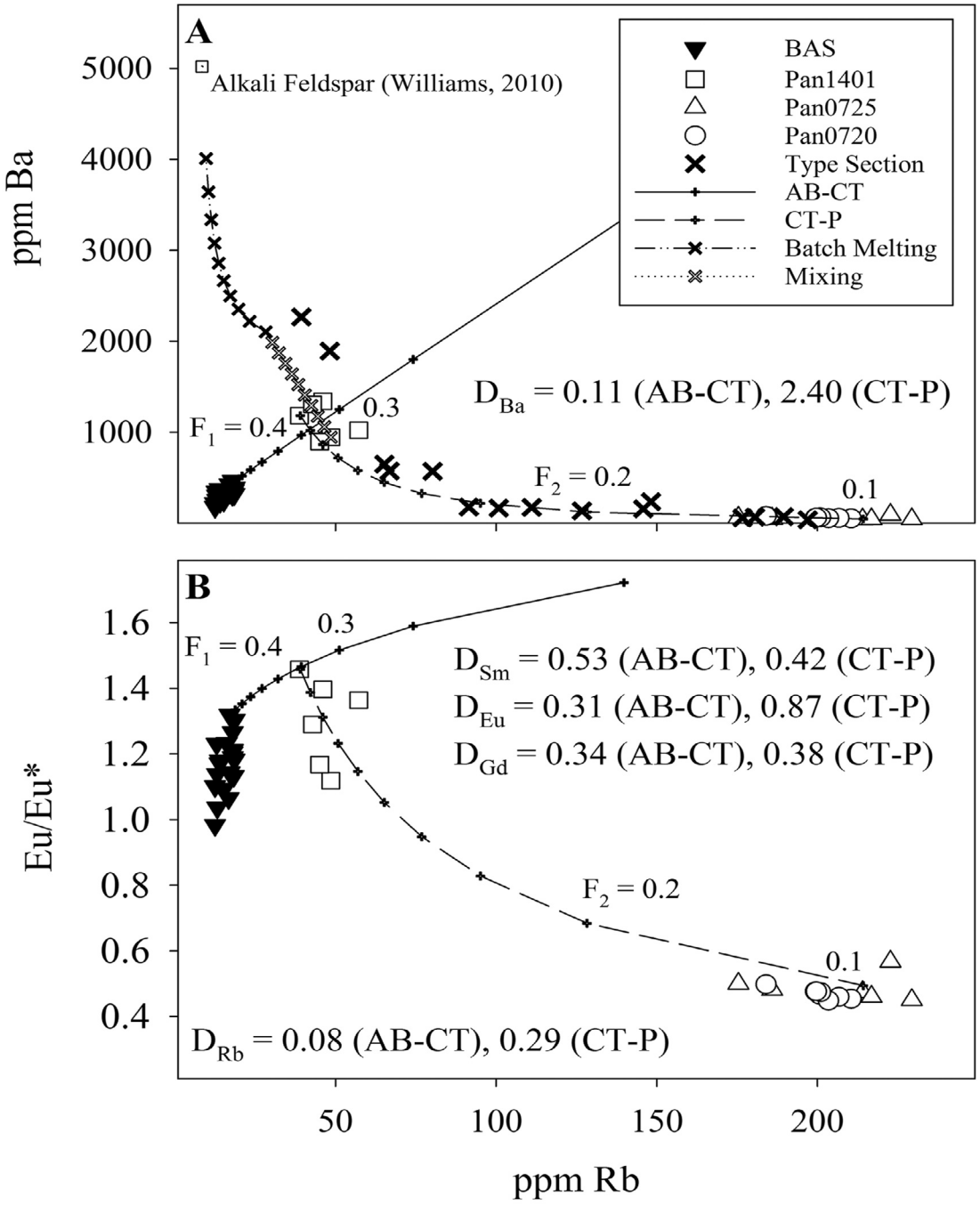

FIGURE 6. (A) Trace-element models of fractional crystallisation for alkali basalt to comenditic trachyte (AB-CT) and comenditic trachyte to pantellerite (CT-P). Bulk partition coefficients are calculated from calculated mineral proportions (Table 2) and mineral/melt coefficents from Neave et al., [2012] (AB-CT) and Mahood and Stimac [1990] (CT-P). F1 = liquid fraction, AB-CT; F2 = liquid fraction, CT-P. (B) Eu/Eu* = EuN/√(SmN·GdN), normalised to CI chondrite following McDonough and Sun [1995]. Whole-rock basalt data (BAS) adapted from Civetta et al., [1998] and White et al., [2009]. Type Section and Alkali Feldspar compositions are adapted from whole-rock data for the GT type locality [Williams, 2010].

teria of Bacon and Hirschmann [1988], which result in Andersen and Lindsley [1988] temperatures and log oxygen fugacities of: (i) 958°C , -12.9 (# 1401-11), (ii) 968°C -12.7 (# 1401-3ter), (iii) 983°C , -12.5 (# 1401-3), and (iv) 1072°C , -1.27 (# 1401-3bis).

Oxygen fugacities for each pair are approximately 1.3 log units below the fayalite-magnetite-quartz buffer (FMQ-1.3) at pressures of 1000 bar [Frost et al., 1988].

Temperatures recovered by QUILF95 [Andersen et al., 1993] are slightly lower, yielding an olivine-clinopyroxene value of 939°C at 1000 bar and silica activity relative to quartz saturation of 0.784. The addition of il-

menite and magnetite to the assemblage also provides log oxygen fugacities of -13.0 (FMQ-1.1)

The H_2O content determined in melt inclusions of the trachytic sample ranges from 0.15 to 1.08 wt% (Table 3). Recent crystallisation experiments on GT trachyte bulk rock composition [Romano, 2017; Romano et al., 2018] provide evidence that the mineral assemblage of natural trachyte of the GT can be reproduced at P = 1.5-1.0 kbar, T = 900-950°C and melt H_2O between 2.5 and 3.0 wt%, at a crystallinity close to 30 wt%. The apparent discrepancy between H_2O content experimentally determined by Romano et al. [2018] and the low-H2O measured in MIs, could be explained if the cpx-hosted MIs have trapped near-liquidus melts. Multiply-saturated melts reproduced in crystallisation experiments indeed were higher in H_2O, due to their higher crystallinity that results in an obvious increase in H_2O_{melt}.

The chlorine content of MIs from the pantelleritic vitrophyre (# Pan0725) is in the range 0.9-1.1 wt%, i.e. within the same range of Cl concentration reported by Lanzo et al. [2013] for MIs and groundmass glasses from the opening pumice fallout, giving a storage pressure of 0.5 kbar for the pre-eruptive pantellerite magma.

7.3 MELTS MODELLING OF THE LIQUID LINE OF DESCENT

The fractional crystallisation model and the pre-eruptive magma conditions were also checked with rhyolite-MELTS program, version 1.1 [Gualda et al., 2012], again using Pan1401 (46) 1 as the model parent. Models were produced for pressures between 500-2000 bar with starting H_2O contents between 0.5-4.0 wt%. Oxygen fugacity for all models was buffered at FMQ - 1, consistent with our geothermometry and the results of White et al. [2005, 2009]. In all models, it was necessary to suppress olivine as a fractionating phase to mimic the liquid line of descent.

Results for all models indicate that alkali feldspar and ilmenite are the first two phases to crystallise, and fractionation of these phases can account for the variability within the comenditic trachyte melt inclusions. Initial melt water content was found to have the largest effect on the temperature of clinopyroxene saturation, with higher values resulting in lower temperatures, but at a given water content the calculated liquid lines of descent are nearly identical, differing only in terms of temperatures of crystallisation and fluid exsolution. Under saturated conditions (~3.8 wt% H_2O), ilmenite is the predicted liquidus phase at 979°C, and is later joined by alkali feldspar (Or_{45}, 869°C) then clinopyroxene (824°C). With lower initial water contents (1.0 wt% H_2O), alkali feldspar (Or_{25}) is the predicted liquidus phase at 994°C, followed by ilmenite (979°C), clinopyroxene (899°C), and aenigmatite (802°C). In plots of FeOt vs. Al_2O_3, P.I., and CaO (Figure 7) changes in slope at $FeO_t \approx 7$ wt% are very likely due to the onset of fractionation of clinopyroxene, with the sudden increase in P.I. providing an example of the "*clinopyroxene effect*" described by Scaillet and Macdonald [2003].

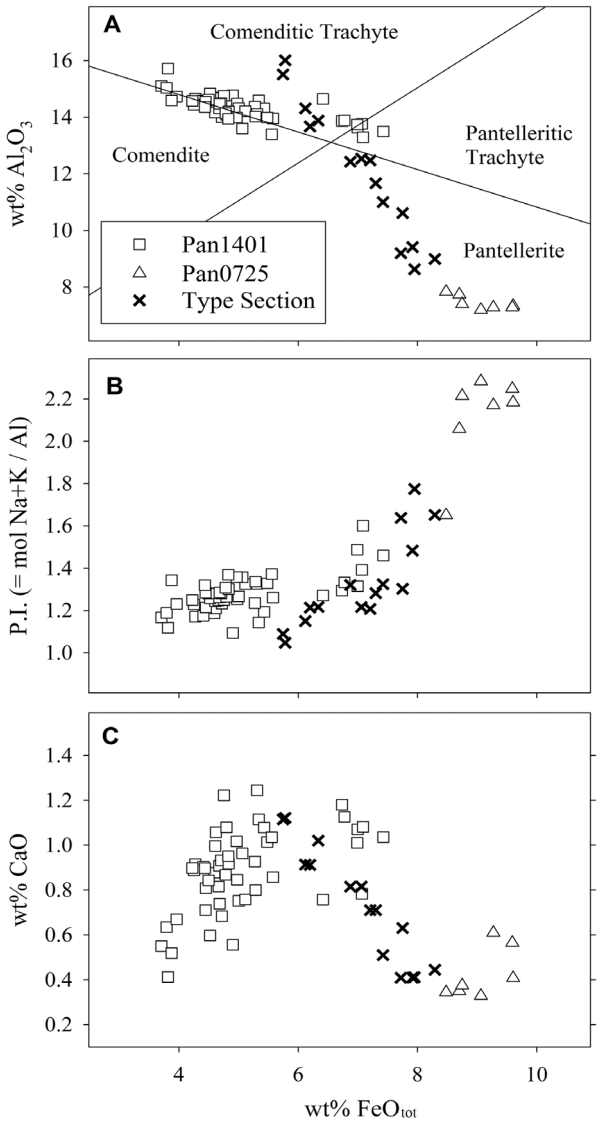

FIGURE 7. FeO_{tot} plotted versus (A) Al_2O_3 [Macdonald, 1974], (B) P.I., and (C) CaO for melt inclusion and whole-rock data from the type section [Williams, 2010]. Elevated Al_2O_3 at low FeO_{tot} may provide additional evidence for feldspar accumulation/resorption in the whole-rock comenditic trachytes (see Figure 6). Changes in slope at ~7 wt% FeO_{tot} may mark the beginning of clinopyroxene fractionation.

7.4 VOLCANOLOGICAL AND PETROLOGICAL INFERENCES

Melt inclusions in the Green Tuff record a change in volatile concentration from ~1.2 wt% H2O in the lower trachyte unit to ~4.2 % H_2O in the upper pantelleritic pumice unit [cf. Lanzo et al., 2013]. Results from previous works on both natural samples and experimental petrology suggest a temperature gradient from ~950°C at the base to <730°C at the top [White et al., 2005, 2009; Di Carlo et al., 2010, Romano et al., 2018]. It is notable that this apparent bottom-to-top increase in H2O and decrease in temperature (ΔT>220°C) is accompanied by a decrease in phenocryst abundance (~30 to <10 vol%), which has been observed in other compositionally zoned silicic magma chambers and attributed to pre-eruptive enrichment of volatile components toward the cooling surface of the magma chamber [Hildreth, 1981]. Similarly zoned magma chambers have been reported for the Laacher See phonolite (2-5 wt% H_2O, ΔT≈80°C), Tenerife phonolite (1.7-5 wt% H_2O, ΔT≈110°C), Fogo A trachyte (1.8-6.5 wt% H_2O, ΔT≈35°C), Xaltipan andesite-rhyolite (0.4-5.2 wt% H_2O, ΔT≈185°C), the Bishop Tuff high silica-rhyolite (4.2-5.7 wt% H_2O, ΔT≈65°C) and others [Wolff et al., 1990].

This apparent water concentration gradient, increasing from trachyte to pantellerite, can be possibly explained by three different processes: (i) post-entrapment diffusive H_2O loss from the analysed melt inclusions; (ii) the trachyte magma was water-undersaturated, although this possibility is in contrast with both crystallisation experiments (see section 7.2) and thermodynamic models [White et al., 2009], and also needs a considerable amount of water to be lost during magma cooling-evolution to originate the trachyte by protracted fractional crystallisation from basalt (H_2O content in MI of basalts is ≤ 1.6 wt %, Gioncada and Landi 2010]; (iii) H_2O exsolution due to increasingly higher feldspar crystallisation (i.e. 2nd boiling) and consequent water migration upwards in the less crystallised pantelleritic portions of the magma chamber. Kennedy [1955] suggested that dissolved water will diffuse towards the lower-temperature and pressure top of the magma chamber to equalise the chemical potential throughout the system, a mechanism endorsed by Hildreth [1981]. Exsolution may occur through "second boiling" in magma chambers - result of prolonged cooling and crystallisation – and this increases pressure in the chamber (because the surrounding country rocks are relatively incompressible) and may trigger eruptions [Tait et al., 1989; Edmonds and Wallace, 2017].

8. CONCLUSIONS

The Green Tuff ignimbrite inundated the whole island of Pantelleria with crystal-poor pantellerites and, at the end of the eruption, with a crystal-rich trachyte, which flowed in a pyroclastic density current in the south-west sector of the island. The chemical zoning of the GT represents a good example of dynamics of relatively low-volume (≤ 1 km^3 DRE) peralkaline silicic magma chamber, very likely fed by a parental basaltic magma.

The study of trace elements and volatile contents in MIs from the chemically most representative portions of the GT, allowed us to settle the following conclusions:

1) clinopyroxene-hosted melt inclusions from the late-erupted trachyte crystal-rich ignimbrite member, caught two different groups that differ in some incompatible elements (in particular, Ba, Eu/Eu*): (i) *low-Ba MIs*, likely derived by FC from a parental basalt, and a (ii) *high Ba MIs*, for which we consider that they represent evolved melts, although we cannot exclude that were captured some amounts of local melts due to feldspar mush partial dissolution.
2) The volatile contents of MIs from the whole Green Tuff sequence reflect an-H_2O-rich top magma chamber (the early tapped pantellerite portions) grading in an H_2O-poor bottom (the late erupted crystal-rich trachyte). One interpretation is that trachyte magma at near-liquidus conditions tracked by cpx-hosted MIs, was water-undersaturated, possibly due to exsolution and vesiculation of an aqueous phase.
3) The results of major- and trace-element modelling are consistent with previous workers [Civetta et al., 1998; White et al., 2009; Neave et al., 2012] who concluded that the basalt-trachyte-pantellerite sequence is the result of extensive fractional crystallisation. Our results suggest that the comenditic trachyte represented by the melt inclusions may form after ~65% crystallisation of an assemblage dominated by plagioclase and clinopyroxene from alkali basalt, and that pantellerite forms after an additional 90% crystallisation of an assemblage dominated by alkali feldspar (for a total of ~97% fractional crystallisation of basalt). In this suite, the maximum Ba concentration through fractional crystallisation

processes is ~1300 ppm, and values in trachytes higher than this are strongly suggestive of feldspar accumulation and resorption processes. Within the comenditc trachyte-to-pantellerite sequence, alkali feldspar plays the major role in driving the liquid line of descent.

REFERENCES

Andersen, D.J., D.H. Lindsley, and P.M. Davidson (1993). QUILF: a PASCAL program to assess equilibria among Fe–Mg–Mn–Ti oxides, pyroxenes, olivine, and quartz, Comp. and Geosc., 19, 1333–1350.

Bacon, C.R. and M.M. Hirschmann (1988). Mg/Mn partitioning as a test for equilibrium between coexisting Fe–Ti oxides, Am. Mineral., 73, 57-61.

Calanchi, N., P. Colantoni, P.L. Rossi, M. Saitta and G. Serri (1989). The Strait of Sicily continental rift systems: physiography and petrochemistry of the submarine volcanic centres, Mar. Geol., 57, 55-83.

Catalano, S., G. De Guidi, G. Romagnoli, S. Torrisi and L. Tortorici (2008). The migration of plate boundaries in the SE Sicily: influence of the large-scale kinematic model of African promontory in southern Italy, Tectonophysics, 449, 41-63.

Civetta, L., M. D'Antonio, G. Orsi and G.R. Tilton (1998). The geochemistry of volcanic rocks from Pantelleria island, Sicily channel:petrogenesis and characteristics of the mantle source region, J. Petrol., 39, 1453-1491.

Civile, D., E. Lodolo, L. Tortorici, G. Lanzafame and G. Brancolini (2008). - Relationships between magmatism and tectonics in a continental rift: The Pantelleria Island region (Sicily Channel, Italy), Mar. Geol., 251, 32-46.

Di Carlo, I., S.G. Rotolo, B. Scaillet, V. Buccheri and M. Pichavant (2010). Phase equilibrium constraints on pre-eruptive conditions of recent felsic explosive volcanism at Pantelleria Island, Italy, J. Petrol., 51, 2245-2276.

Dixon, J.E., E.M. Stolper,. and J.R. Holloway (1995). An experimental study of water and carbon dioxide solubilities in mid-ocean ridge basaltic liquids. Part I: calibration and solubility models, J. Petrol., 36, 1607–1631.

D'Oriano, C., P.Landi, A. Pimental and V. Zanon (2017). Magmatic processes revealed by anorthoclase textures and trace element modeling: The case of the Lajes Ignimbrite eruption (Terceira Island, Azores), J. Volcanol. Geoth. Res., 347, 44-63.

Edmonds, M. and P. J. Wallace (2017). Volatiles in volcanic systems. Elements 13, 29-33.

Ferla, P. and C. Meli (2006). Evidence of magma mixing in the "Daly Gap" of alkali suites: a case study from the enclaves of Pantelleria (Italy), J. Petrol., 47, 1467-1507.

Frost, B.R., D.H. Lindsley and D.J. Andersen (1988). Fe–Ti oxide–silicate equilibria: assemblages with fayalitic olivine, Am. Mineral., 73, 727–740.

Gioncada, A. and P. Landi (2010). The pre-eruptive volatile contents of recent basaltic and pantelleritic magmas at Pantelleria (Italy), J. Volcanol. Geoth. Res., 189, 191-201.

Gualda, G. A. R., M.S. Ghiorso, R.V Lemons and T.L. Carley (2012). Rhyolite-MELTS: a modified calibration of MELTS optimized for silica-rich, fluid-bearing magmatic systems, J. Petrol, 53, 875–890.

Hildreth, W. (1981). Gradients in silicic magma chambers: Implications for lithospheric magmatism, J. Geophys. Res., 86, 10153-10192.

Jordan, N.J., S.G. Rotolo, R. Williams, F. Speranza, WC. McIntosh, M.J, Branney and S. Scaillet (2018). Explosive eruptive history of Pantelleria, Italy: repeated caldera collapse and ignimbrite formation at a peralkaline volcano, J. Volcanol. Geoth. Res., 349, 67-73.

Kennedy, G.C. (1955). Some aspects of the role of water in rock melts, Geol. Soc. Am. Sp. Pap., 62, 489-504.

Lanzo, G., P. Landi, and S.G. Rotolo (2013). Volatiles in pantellerite magmas: a case study of the Green Tuff Plinian eruption, J. Volcanol. Geoth. Res., 262, 153-163.

Lowenstern, J.B., 1994. Chlorine, fluid immiscibility, and degassing in peralkaline magmasfrom Pantelleria, Italy, Am. Mineral., 79, 353–369.

Lowenstern, J.B. and G.A. Mahood (1991). New data on magmatic H2O contents with implications for petrogenesis and eruptive dynamics at Pantelleria, Bull. Volcanol., 54, 78-83.

McDonough, W.F. and S. Sun (1995). Composition of the Earth, Chem Geol., 120, 223-253.

Mahood, G.A. and W. Hildreth (1986). Geology of the peralkaline volcano at Pantelleria, Strait of Sicily, Bull. Volcanol., 48, 143-172.

Mahood, G.A. and J.A Stimac (1990). Trace-element partitioning in pantellerites and trachytes,

Geochim. Cosmochim. Acta., 54, 2257-2276.

Métrich, N., J. Susini, E. Foy, F. Farges, D. Massare, L. Sylla, S. Lequien and M. Bonin-Mossba (2006). Redox state of iron in peralkaline rhyolitic glass/melt X-ray absorption micro-spectroscopy experiments at high temperature, Chem. Geol. 231, 350-363.

Neave, D.A., G. Fabbro, R.A. Herd, C.M Petrone. and M. Edmonds (2012). Melting, differentiation and degassing at the Pantelleria volcano, Italy, J. Petrol., 53 637-663.

Romano, P. (2017). Experimental investigation on peralkaline silicic magmas of Pantelleria Island: inferences on pre-eruptive conditions, magma evolution and water solubility, PhD thesis, University of Palermo.

Romano, P., J. Andújar, B. Scaillet, N. Romengo, I. Di Carlo and S.G. Rotolo (2018). Phase equilibria of Pantelleria trachytes (Italy): Constraints on pre-eruptive conditions and on the metaluminous to peralkaline transition in silicic magmas. J. Petrol., in press, doi: 10.1093/petrology/egy037.

Rotolo, S.G., F. Castorina, D. Cellura and M. Pompilio (2006). Petrology and Geochemistry of submarine volcanism in the Sicily Channel Rift, J. Geol., 114/3 355-365.

Scaillet, B. and R. Macdonald (2001). Phase relations of peralkaline silicic magmas and petrogenetic implications, J. Petrol., 42, 825-845.

Scaillet, B. and R. Macdonald (2003). Experimental constraints on the relationships between peralkaline rhyolites of the Kenya rift valley, J. Petrol., 44, 1867-1894.

Scaillet, B. and R. Macdonald (2006). Experimental and thermodynamic constraints on the sulphur yield of peralkaline and Metaluminous silicic flood eruptions, J. Petrol., 47, 1413-1437.

Scaillet, S., G. Vita-Scaillet and S. G. Rotolo (2013). Millenial-scale phase relationships between ice-core and Mediterranean marine records: insights from high-precision 40Ar/39Ar dating of the Green Tuff of Pantelleria, Sicily Strait. Quat. Sci. Rev., 78, 141-154.

Tait, S., C. Jaupart and S. Vergniolle (1989). Pressure, gas content and eruption periodicity of a shallow, crystallizing magma chamber, Earth Planet. Sci. Lett., 92(1), 107–123.

White, J.C., D.F. Parker and M. Ren (2009). The origin of trachyte and pantellerite from Pantelleria, Italy: insights from major elements, trace elements, and thermodynamic modelling, J. Volcanol. Geoth. Res., 179, 33-55.

Williams, R., (2010). Emplacement of Radial Pyroclastic Density Currents Over Irregular Topography: The Chemically-zoned, Low Aspect-ratio Green Tuff Ignimbrite, Pantelleria, Italy, University of Leicester, https://doi.org/10.6084/m9.figshare.789054.v1 PhD thesis.

Williams, R., M.J. Branney and T.L. Barry (2014). Temporal and spatial evolution of a waxing then waning catastrophic density current revealed by chemical mapping. Geology, 42, 107–110.

Wolff, J.A., G. Görner and S. Blake (1990). Gradients in physical parameters in zoned felsic bodies: implications for evolution and eruptive withdrawal, J. Volcanol. Geoth. Res., 43, 37-55.

CORRESPONDING AUTHOR: Pierangelo ROMANO,
Dipartimento Scienze della Terra e del Mare (DiSTeM),
Università degli Studi di Palermo
Palermo, Italy
email: pierangeloromano@gmail.com